Article

Effects of Metal#Molecule Contact and Molecular Structure on Molecular Electronic Conduction in Nonresonant Tunneling Regime: Alkyl versus Conjugated Molecules

Gunuk Wang, Tae-Wook Kim, Yun Hee Jang, and Takhee Lee

More About This Article

Additional resources and features associated with this article are available within the HTML version:

- Supporting Information
- Access to high resolution figures
- Links to articles and content related to this article
- Copyright permission to reproduce figures and/or text from this article

View the Full Text HTML

Effects of Metal−Molecule Contact and Molecular Structure on Molecular Electronic Conduction in Nonresonant Tunneling Regime: Alkyl versus Conjugated Molecules

Gunuk Wang, Tae-Wook Kim, Yun Hee Jang, and Takhee Lee*

Department of Materials Science and Engineering, Gwangju Institute of Science and Technology, Gwangju 500-712, Korea

Received: June 3, 2008

The effect of metal−molecule contacts and molecular structures on the electronic conduction of alkyl and conjugated molecular junctions in nonresonant tunneling regime was investigated based on a proposed multibarrier tunneling (MBT) model, where the molecular junction was decomposed into three individual barriers through the molecular body and metal−molecule contacts on either side of the molecule. The resistance−area product (R_A), specific contact resistance (R_C), and decay coefficients (β_C, β_P, β_{Body}, and β_o) were estimated for alkyl and two selected conjugated molecules (oligoacene and oligophenylene) between Au contacts, and the result of R_A (alkyl) > R_A (oligoacene) $\geq R_A$ (oligophenylene) for a given molecular length was obtained from different decay coefficients for different molecules. By assuming the tunneling around the highest occupied molecular orbital of alkyl molecules (like a hole type tunneling), R_C for alkanemonothiol and alkanedithiol junctions with various metallic (Ag, Cu, and Au) contacts was observed to decrease when metal work function was increased.

Introduction

Molecular electronics with an idea of using molecules as functional electronic device components has demonstrated promises for application such as ultrahigh-density memory circuits as alternatives to high-cost silicon-based integrated devices.[1–4] However, the molecular electronics also face many challenges to be overcome for further realization of such device applications, for example, the charge transport mechanism should be understood before any of the device applications.[4] There have been intensive studies on the charge transport properties for basic molecular systems;[5–12] however, functional molecules having shown memory or switching behaviors have not been thoroughly understood in terms of the operation mechanisms.[3] In addition, molecular devices have exhibited relatively poor device-to-device uniformity, short lifetime in device functions, and device instability upon exposure to ambient or to higher temperature environments.[11–15] Particularly, the metal−molecule interface is not well controlled, which is responsible for the stability, reproducibility, and uniformity of molecular devices.[3,11–15] For this reason, the deeper understanding of the influence of metal−molecule contacts on the charge transport behavior in various metal−molecule−metal (M−M−M) junctions is of great importance for the further development of molecular electronic device applications.

Here we report on the charge transport properties of metal−molecule contacts and molecular structure for M−M−M junctions of alkyl molecules versus conjugated molecules, using our previously proposed multibarrier tunneling (MBT) model. In the MBT model, a metal−molecule−metal junction is divided into three parts: a molecular body region and metal−molecule contacts on either side of molecule. Particularly in our study, we compared the electronic transport properties such as resistance, specific contact resistance, and decay coefficients for a few selected aliphatic (alkyl) and conjugated (oligoacene and

SCHEME 1: The molecular structures and reported molecular body decay coefficients for aliphatic (1, alkyl) and conjugated molecules (2, oligoacene and 3, oligophenylene) in Au−molecule−Au junctions

	Molecule	Molecular structure unit	β_{Body} (Å^{-1})
Monothiol	1		0.93 ± 0.03 [15]
	2		0.50 ± 0.09 [19]
	3		0.42 ± 0.07 [20]
Dithiol	1		0.92 ± 0.08 [15]
	2		
	3		

oligophenylene) molecular junctions with different molecular lengths and different metal electrodes (e.g., Ag, Cu, and Au).

Experimental Section

Preparation of Self-assembled Monolayers. Two types of alkanethiol self-assembled monolayers (SAMs), alkanemonothiols and alkanedithiols, were prepared. These two types have the same molecular structures (shown as "1" in Scheme 1) and are distinguished by the nature of metal−molecular contacts when they are sandwiched between metal contacts in M−M−M junctions. Three different lengths of molecules were used for each type of alkanethiol SAMs. Octanemonothiol ($CH_3(CH_2)_7$-SH, denoted as C8 for the number of alkyl units), dodecanemonothiol ($CH_3(CH_2)_{11}SH$, C12), and hexadecanemonothiol ($CH_3(CH_2)_{15}SH$, C16) were used for alkanemonothiols (from Aldrich Chemical Co.), and octanedithiol ($HS(CH_2)_8SH$, DC8), nonanedithiol ($HS(CH_2)_9SH$, DC9), and decanedithol ($HS(CH_2)_{10}SH$, DC10) were used for alkanedithiols (from Tokyo Chem. Industry). To make molecular solutions, ~5 mM

Electronic Conduction in Nonresonant Tunneling Regime

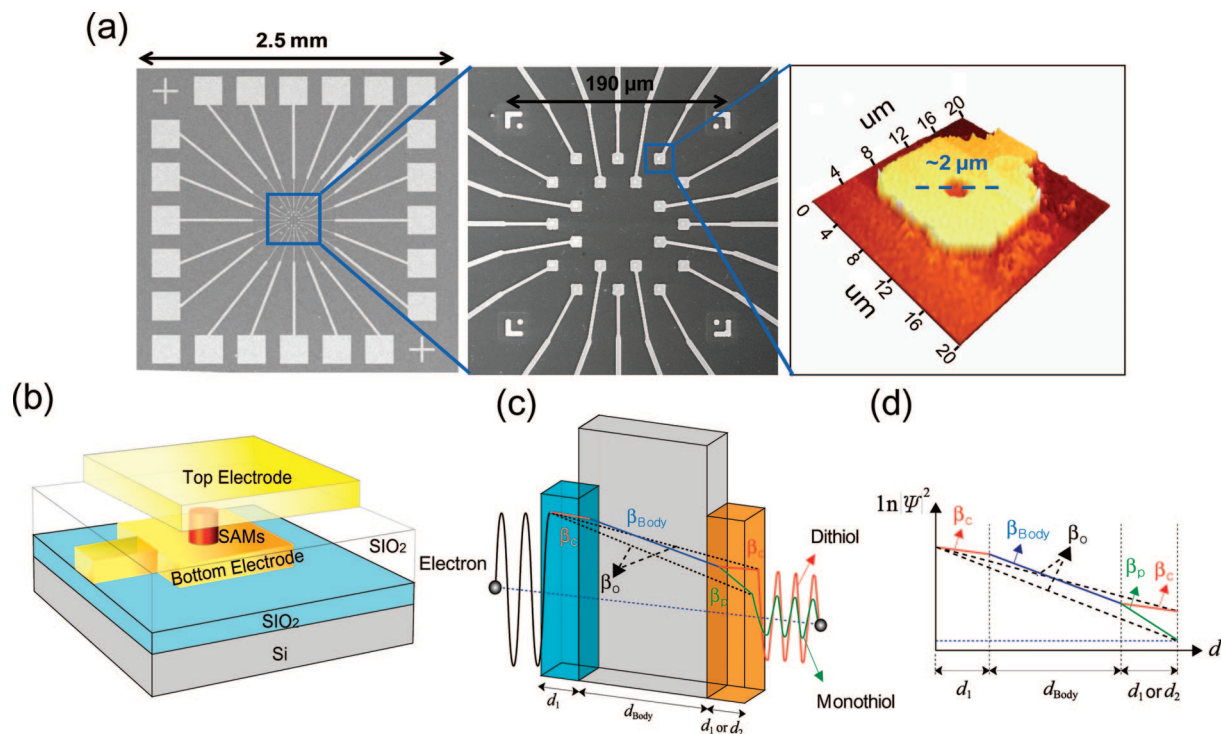*J. Phys. Chem. C, Vol. 112, No. 33, 2008* **13011**

Figure 1. (a, left and center) SEM images of a fabricated M−M−M device without top electrode, (right) AFM image of a molecular junction with a cross-sectional profile across the junction. (b) Schematic of the vertical M−M−M device with a microscale via-hole junction. (c) Illustration of the MBT model. (d) Schematic of the MBT model for a molecular M−M−M junction. The width of the barrier d_{Body} represents the length of the molecular body corresponding to the molecular body decay coefficient (β_{Body}), as illustrated by the blue line. The widths of the barrier for $d_{1(2)}$ represent the length of the contact corresponding to the contact decay coefficients (β_C, β_P), that is, chemisorbed contact d_1 (β_C) [metal−S-C] and physisorbed contacts d_2 (β_P) ([CH₃/metal] or [H/metal], as illustrated by the red and green lines, respectively. The β_o are the overall decay coefficients through the overall molecular tunnel barriers for monothiol and dithiol, as illustrated by the black dashed lines.

alkanethiol solutions were made by adding ∼10 μL of alkanethiols to ∼10 mL of anhydrous ethanol (from Aldrich Chem. Co.).

Fabrication of Metal−Molecule−Metal Junction Devices. The alkanethiol (alkanemonothiol and alkanedithiol) metal−molecule−metal (M−M−M) junction devices were fabricated on a p-type (100) Si substrate covered with a thermally grown 3000 Å thick layer of SiO₂. The conventional optical lithography method was used to pattern bottom electrodes that were prepared with Au (1000 Å)/Ti (50 Å) using an electron beam evaporator. A SiO₂ layer (700 Å thick) was deposited on the patterned bottom by plasma enhanced chemical vapor deposition. Reactive ion etching (RIE) was then performed to create microscale via-holes of 2 μm diameter through the SiO₂ layer to expose the Au surfaces of the bottom electrodes. The chips were left in the molecular solutions for 24−48 h for the alkanethiol SAMs to assemble on the Au surfaces exposed by RIE in a nitrogen-filled glovebox with an oxygen level of less than ∼10 ppm. After the alkanethiol SAMs were formed on the exposed Au surfaces, a top Au electrode was made by thermal evaporation to form M−M−M junctions. This evaporation was done with a shadow mask on the chips with a liquid nitrogen cooled cold stage in order to minimize thermal damage to the active molecular component under a pressure of ∼10⁻⁶ Torr. For the same reason, the deposition rate for the top Au electrode was kept very low, typically ∼0.1 Å/s until the total thickness of the top Au electrode reached ∼500 Å.

Imaging and Electrical Characterizations. M−M−M junction devices were characterized with scanning electron microscopy (TESCAN, VEGA model) and atomic force microscopy (PSIA, XE-100 model). Figure 1a shows a series of SEM images

and AFM image of the fabricated M−M−M devices before the top electrode metallization, and Figure 1b shows the schematic diagram of a molecular device. In the fabrication of our molecular devices, a 1 × 1 cm unit piece contains 16 dies (a die is shown in the left picture in Figure 1a), and each die contains 20 individual molecular M−M−M devices (middle picture in Figure 1a); thus, each unit piece has a total of 320 molecular devices. The room temperature current−voltage (I−V) characteristics of all of the fabricated devices were evaluated using a semiconductor parameter analyzer (HP4155A).

Theoretical Basis

Multibarrier Tunneling Model. Previously, we have reported on the charge transport properties of metal−molecule contacts for alkyl molecular junctions using a proposed MBT model[15] that generalizes the Simmons tunneling model,[16] a widely used model for describing a rectangular tunneling barrier. This rectangular-shaped barrier (trapezoidal-shaped barrier with bias applied) turns to a triangular shaped barrier when the applied bias exceeds the barrier height (Fowler−Nordheim tunneling). When the Fermi level of the metal is aligned close enough to one energy level such as highest occupied molecular orbital (HOMO), the Simmons model is a good approximation,[6,11,15,16] because the effect of the other distant energy level, lowest unoccupied molecular orbital (LUMO), on the tunneling transport is negligible.[17] As compared to the Simmons tunneling model, where the tunneling barrier is represented by a single barrier, the MBT model decomposes the charge transport through an M−M−M junction into individual transport through a molecular body and metal−molecule contacts on either side of the molecule,[15]

as schematically illustrated in Figure 1c. This approach of separating the metal−molecule contacts and molecular body region in an M−M−M junction is valid when nonresonant tunneling is the main conduction mechanism of the electronic charge transport particularly at a relatively low bias regime. Note that when the applied bias is much smaller than the HOMO−LUMO gap and the barrier height (Fermi energy − HOMO in most cases for a hole-type transport[17]), the electronic transport can be considered as nonresonant tunneling, that is, the transport is mainly dominated by the quantum mechanical tunneling.[18] These conditions are well satisfied for the alkyl molecular junctions because the Fermi level of the metal electrodes falls within the HOMO−LUMO gap of the alkyl molecules (∼8 eV) and the main conduction mechanism is nonresonant tunneling at a low bias.[6] Note that although the validity conditions of the MBT model can also be satisfied for some conjugated molecule,[19,20] normally the MBT model is not applicable to conjugated molecules having relatively small HOMO−LUMO gap and especially in high bias regime because of the onset of transport through resonant states of the molecules hybridized with the metal electrodes,[17b,21] where the separation of metal−molecule contacts and molecular body from the molecular junction may not be valid. A few previous theoretical and experimental studies[17b,21] on conjugated molecules have found a region of lower differential conductance (weak hybridization) at low bias and a strong increase in the differential conductance at higher biases due to the onset of transport through resonant states of the molecule hybridized with the metal electrodes.

In this study, we focus on the low bias regime (nonresonant tunneling regime) to deduce important transport properties such as resistance−area product (R_A), specific contact resistances (R_C), and decay coefficients for alkyl and two selected conjugated molecules (oligoacene and oligophenylene, shown as "2" and "3" in Scheme 1, respectively) with various metal contacts based on the MBT model. Here, the low bias was somewhat arbitrarily defined. For example, −0.3 V < V < 0.3 V has been used for the low bias range in studying charge transport for alkyl, oligophenylene, and oligoacene molecular systems.[19,20,22] We adopt similar bias range for the low bias regime in our study. In the low bias regime, the tunneling current density can be approximated as follows,[16]

$$J \approx \frac{(2m\Phi_B)^{1/2}e^2\alpha}{4\pi^2\hbar^2 d}V\exp\left[-\frac{2(2m)^{1/2}}{\hbar}\alpha(\Phi_B)^{1/2}d\right] \quad (1)$$

$$\beta_o = \frac{2(2m)^{1/2}}{\hbar}\alpha(\Phi_B)^{1/2} \quad (2)$$

where m is the electron mass, d is the total barrier width or molecular length, Φ_B is the rectangular barrier height at zero bias, e is the electronic charge, V is the applied bias, and α is a unitless adjustable parameter introduced to modify the simple rectangular barrier model or to account for the effective mass of the tunneling electrons through a rectangular barrier. β_o is the overall decay coefficient in the low bias regime, which reflects the degree of decrease in wave function of the tunneling electron through the overall molecular tunnel barrier.[15] A higher decay coefficient implies a faster decay of the wave function, that is, lower electron tunneling efficiency. In the MBT model, it is possible to describe the overall slope of wave function decay through the barriers based on the magnitude of the β_o value, and this overall decay can be further decomposed to three individual decays through three individual barriers, that is,

barriers corresponding to the molecular body and metal−molecule contacts on either side of the molecule, as shown in Figure 1c. Then, the overall decay coefficient β_o can be expressed as eq 3 for monothiol (dithiol) junctions from consideration of geometric configurations (Figure 1, panels c and d).

$$\beta_o = (\beta_C d_1 + \beta_{Body}d_{Body} + \beta_{C(P)}d_{1(2)})/(d_1 + d_{Body} + d_{1(2)}) \quad (3)$$

where $\beta_{C(P)}$ is the chemisorbed (physisorbed) contact decay coefficient corresponding to the chemisorbed (physisorbed) contact width d_1 (d_2), β_{Body} is the decay coefficient component for the molecular body width d_{Body}, as illustrated in Figure 1, panels c and d. Also, $\alpha(\Phi_B)^{1/2}$ can be expressed as eq 4 by combining eq 2 and eq 3.

$$\alpha(\Phi_B)^{1/2} = \frac{\hbar}{2(2m)^{1/2}}\frac{\beta_C d_1 + \beta_{Body}d_{Body} + \beta_{C(P)}d_{1(2)}}{d_1 + d_{Body} + d_{1(2)}} \quad (4)$$

Note that because the main conduction mechanism is nonresonant (coherent) tunneling at low bias (and at room temperature), it is assumed that the energy of electron tunneling through the molecular barriers does not decrease, as expressed by the horizontal blue dashed line in panels c and d of Figure 1. The electron transmission for the chemisorbed contact [metal−S−C] was found to be more efficient than that for physisorbed contact [CH₃/metal] or [H/metal] (i.e., $\beta_C < \beta_P$), as summarized in Table S1 in the Supporting Information and expressed as different slopes for β_C (red line) and β_P (green line) in Figure 1, panels c and d. As a result, the β_o values for monothiol junctions are larger than those for dithiol junctions, that is, the slope for the wave function decay through monothiol junctions is more steep than that for the case of dithiol junctions, as shown in panels c and d of Figure. It has been found that the chemisorbed contact decay coefficient (β_C) and physisorbed contact decay coefficient (β_P) are ∼0.05 and ∼1.89 Å⁻¹, respectively, corresponding to a chemisorbed contact barrier [Au−S−C] and physisorbed contact barrier [CH₃/Au] or [H/Au], respectively.[15] The β_{Body} values listed in Scheme 1 are shown to be dependent on the molecular structure but not quite on the metal−molecule contact in the nonresonant tunneling regime, which suggests that the Fermi level is too far from the molecular energy level to substantially impact β_{Body}.[15,19,20,22] Kim et al. have found that the difference in HOMO positions for thiol (−S) and isocyanide (−NC) oligoacene molecules does not appear to affect the β_{Body} values (0.5 ± 0.09 Å⁻¹ for −S vs 0.49 ± 0.08 Å⁻¹ for −NC),[19] and Engelkes et al. have also found that β (β_{Body} in our notation) values are almost same for alkanemonothiol and alkanedithiol and are independent of metal work functions.[22] Their β (β_{Body} in our notation) value was 0.88 ± 0.08 Å⁻¹, which is consistent with our finding that β_{Body} values were determined to be ∼0.93 ± 0.03 and ∼0.92 ± 0.08 Å⁻¹ for alkanemonothiol and alkanedithiol, respectively, almost identical values for the two molecular systems.[22] Note that β_{Body} values of selected molecular junctions were obtained from the slopes in the semilog plot of resistance R versus the molecular length at a low bias range, as the β_{Body} values summarized in Scheme 1. Also note that, generally, β_o depends on the molecular length, which reflects the different tunneling rates for different lengths of molecule, whereas β_{Body} does not depend on molecular length. This can be understood from the geometrical consideration of Figure 1, panels c and d.[15] (See Figures S5 and S6 in the Supporting Information.)

In the typical nonresonant tunneling case, the resistance is exponentially dependent on the molecular length d (= $d_1 + d_{1(2)}$

Electronic Conduction in Nonresonant Tunneling Regime

J. Phys. Chem. C, Vol. 112, No. 33, 2008 **13013**

+ d_{Body}). The widths of the barrier for d_1, d_{Body}, and d_2 in alkyl molecular system represent the length of the chemisorbed contact on the molecule [Au−S−C], the molecular body region [$(CH_2)_n$], and the physisorbed contact on the molecule [CH_3/ Au], respectively. Here, we assume d_{Body} is the projected length along the molecular body with the incremental length per carbon atom (Δd_{Body} [CH_2]) of ~1.25 Å, and the contact lengths (d_1 and d_2) are the vertical distances between contact sites of molecule and electrode (see details in the Supporting Information, especially Figure S2). The length d_{Body} is identical for *n*-alkanemonothiol and *n*-alkanedithiol with the same *n* value. For example, octanemonothiol (C8) and octanedithiol (DC8) have an identical length, d_{Body} [$(CH_2)_8$, ~8.75 Å], and d_1 ([Au−S−C]) is ~3.2 Å and d_2 ([CH_3/Au]) is ~1.4 Å.

For the case of oligoacene molecules, the width of the barrier for d_2 [H/Au] in the conjugated molecular system is ~1 Å.[20] The total lengths (*d*) for oligoacene thiols are estimated to be ~6.88, ~9.02, and ~11.28 Å for benzenethiol (Ph-S), 2-naphthalenethiol (Naph-S), and 2-anthracenethiol (Anth-S) with one, two, and three units of oligoacene (benzene) structure (*n* = 1, *n* = 2, and *n* = 3), respectively.[19] The total lengths (*d*) for oligophenylene thiols are estimated to be ~8.37, ~12.54, and ~16.71 Å for oligophenylene thiol derivatives with one, two, and three units of oligophenylene (toluene) structure, respectively.[20] Here, all the molecular lengths were estimated with Cambridge Scientific Chem 3D software (See Figure S2 in the Supporting Information).

At low bias, eqs 1 and 3 can be used to determine the resistance (*R*) in the Ohmic regime as follows,

$$R = \frac{4\pi^2\hbar^2}{A(2m)^{1/2}e^2}\left(\frac{d_1 + d_{Body} + d_{1(2)}}{(\Phi_B)^{1/2}\alpha}\right)\exp[\beta_C d_1 + \beta_{Body}d_{Body} +$$
$$\beta_{C(P)}d_{1(2)}] \quad (5)$$

where *A* is a junction area. The contact resistance R_o can be deduced by extrapolating that calculated from eq 5 to a zero molecular-chain body length d_{Body}. Using eqs 4 and 5, the contact resistance R_o can be defined in the limiting case when d_{Body} approaches zero, and is expressed as eqs 6 and 7 for monothiol and dithiol, respectively.

$$R_o = \frac{8\pi^2\hbar}{Ae^2}\left(\frac{(d_1 + d_2)^2}{\beta_1 d_1 + \beta_2 d_2}\right)\exp[\beta_C d_1 + \beta_P d_2] \quad (6)$$

$$R_o = \frac{8\pi^2\hbar}{Ae^2}\left(\frac{2d_1}{\beta_1}\right)\exp[2\beta_C d_1] \quad (7)$$

Similarly, using eq 2, the contact decay coefficients $\beta_{C(P)}$ for Au contacts can be expressed as eq 8,

$$\beta_{C(P)} = \frac{2(2m)^{1/2}}{\hbar}\alpha_{C(P)}(\Phi_{C(P)})^{1/2} \quad (8)$$

where $\Phi_{C(P)}$ is the contact barrier height at zero bias and $\alpha_{C(P)}$ is α values through the contact barrier. These two values can be obtained from α and Φ_B in Au−alkyl molecule contacts, which can be deduced from the molecular body decay coefficients (β_{Body}) and widths (d_1, d_2, d_{Body}) of each barrier part. Note that α and Φ_B values show molecular length dependencies, as shown in Figure S4 in the Supporting Information.

Furthermore, the decay coefficients and specific contact resistance can be determined for molecular junctions with various metal contacts other than Au. If molecular monolayers are sandwiched between other metals (Ag, Cu, and Pd), then the contact barrier heights can be expressed as $\Phi_{C(other\ metals)}$ = $\Phi_{C(Au)}$ + $\Delta\Phi_{(Au-other\ metals)}$ and $\Phi_{P(other\ metals)}$ = $\Phi_{P(Au)}$ +
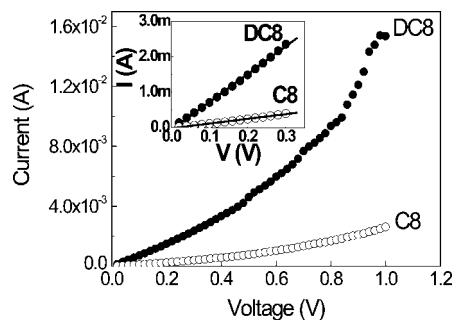

Figure 2. Current−voltage (I−V) characteristics of C8 and DC8 representative devices. Inset plot shows I−V linear fitting for C8 and DC8 at the Ohmic regime.

$\Delta\Phi_{(Au-other\ metals)}$ for chemisorbed contact and physisorbed contact, respectively, by assuming the tunneling around HOMO levels (i.e., a hole-type tunneling). Note that $\Delta\Phi_{(Au-other\ metals)}$ is the difference between the work function of Au and that of the other metal. From eq 8 and using Φ_C, Φ_P, α_C, and α_P, the contact decay coefficient $\beta_{C(P)(Ag\ and\ Cu)}$ can be calculated as {$\beta_{C(Ag)}$ = 0.51 Å^{-1} and $\beta_{C(Cu)}$ = 0.38 Å^{-1}} and {$\beta_{P(Ag)}$ = 2.76 Å^{-1} and $\beta_{P(Cu)}$ = 2.28 Å^{-1}} for chemisorbed contacts and physisorbed contacts, respectively.

Results and Discussion

Figure 2 shows representative current−voltage (I−V) characteristics for DC8 and C8 devices. The resistance of each device was calculated from the linear fitting at the low bias Ohmic regime from 0 to 0.3 V (inset in Figure 2). From the similar linear fittings for all other alkyl molecular devices (Figures S1 in the Supporting Information), we obtained the experimental resistance *R* values of (9.28 ± 4.92) × 10^2, (1.42 ± 0.77) × 10^5, and (1.54 ± 1.25) × 10^7 Ω for C8, C12, and C16, respectively, and (1.15 ± 0.41) × 10^2, (3.98 ± 2.28) × 10^2, and (1.08 ± 0.76) × 10^3 Ω for DC8, DC9, and DC10, respectively. Here, the average *R* values were determined by taking the statistical average of all *R* values obtained by linear fitting of all I−V data for alkyl molecular junctions, and the error values are their standard deviations. The resistance of alkyl molecular junction are clearly dependent on the molecular length and metal−molecular contacts (i.e., monothiol vs dithiol). For example, although C8 and DC8 have an identical molecular body (d_{Body} ([CH_2]$_7$)), the resistance between them is different, specifically, the resistance for C8 is larger than that for DC8 roughly by twice. This different resistance is due to their different natures of metal−molecule contact properties ([CH_3/ Au] versus [Au−S−C]) at Au−molecule contacts.

The resistance *R* can be considered a quantity comparing the transport properties of alkyl versus conjugated molecules. However, since *R* depends on the junction area *A*, the resistance−area product R_A (= *R* × *A*), the junction area-compensated quantity, can be compared among devices with different junction areas and different molecules. Note that the resistance per molecule R_{mol} is more reasonable for molecular footprint than R_A; however, estimation of R_{mol} requires the information of unit cell per molecule that can be accurately found by scanning tunneling microscopy (STM) images. When the accurate information of unit cell per molecule or the number of molecules contained within the junction is not available, one cannot get R_{mol}. Instead, R_A is a good quantity to be compared between different molecular systems (See more discussions in the Supporting Information). The junction areas *A* of molecular
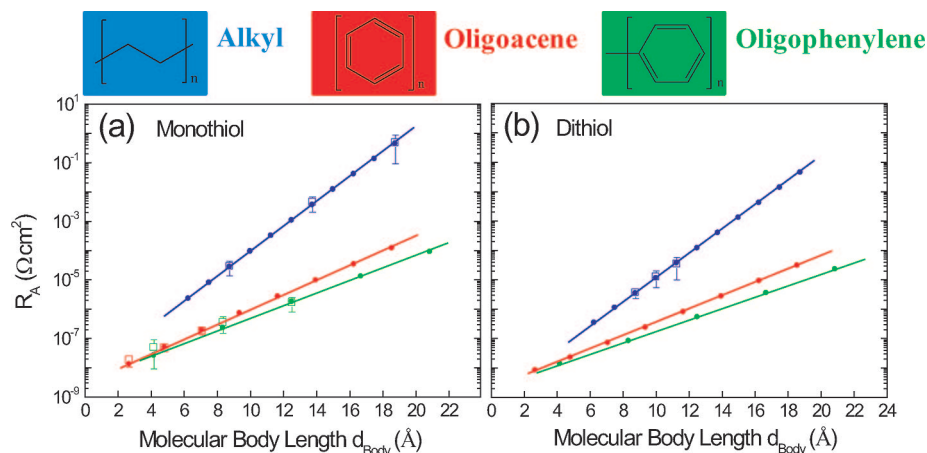
Figure 3. Semilog plots of experimental (open blue squares), reported (open red and green squares),[15,19,20] and calculated R_A values (filled circles) obtained using eq 5 as a function of the molecular body length for (a) monothiol and (b) dithiol junctions for three different molecules [blue (alkyl), red (oligoacene), and green (oligophenylene)] in Au−molecule−Au junctions. The solid lines are the fitting results based on the calculated R_A values using the MBT model.

junctions were estimated as ~3.14 × 10^{-8} cm^2 (2 μm diameter junction devices) for our alkyl molecular devices and 10−15 nm^2 (junction area estimated under conducting atomic microscopy tips)[19,20] for two conjugated molecular (oligophenylene and oligoacene) junctions. Note that our experiment is not based on experiment system for a single molecule such as STM experiment and nanogap device structure. The transport properties values obtained from our experimental results with microscale molecular junctions are an average effect with various microstructures of metal−molecule contacts and binding sites.

Figure 3 shows the R_A values of monothiol and dithiol M−M−M junctions with Au contacts for three different molecular structures (alkyl, oligoacene, and oligophenylene). Figure 3a presents the experimental R_A values (for alkyl), the reported values (for oligoacene and oligophenylene), and the theoretical values calculated using eq 5 at low bias regime. The experimental R_A values for alkyl molecules with Au contacts are (2.91 ± 1.54) × 10^{-5}, (4.46 ± 2.41) × 10^{-3}, and (4.85 ± 3.92) × 10^{-1} Ω cm^2 for C8, C12, and C16, respectively, and (3.62 ± 1.28) × 10^{-6}, (1.25 ± 7.16) × 10^{-6}, and (3.38 ± 2.40) × 10^{-5} Ω cm^2 for DC8, DC9, and DC10, respectively. The estimated R_A values for oligoacene thiols are (1.80 ± 0.75) × 10^{-8}, (4.80 ± 1.20) × 10^{-8}, and (1.80 ± 0.45) × 10^{-7} Ω cm^2 for benzenethiol (Ph-S), 2-naphthalenethiol (Naph-S), and 2-anthracenethiol (Anth-S), respectively.[19] And, the estimated R_A values for oligophenylene thiols are (4.95 ± 4.05) × 10^{-8}, (3.50 ± 2.00) × 10^{-7}, and (1.65 ± 0.85) × 10^{-7} Ω cm^2 for oligophenylene thiol derivatives with one, two, and three units of oligophenylene (toluene) structure, respectively.[20] Using β_C (~0.05 Å^{-1}) and β_P (~1.89 Å^{-1}) values corresponding to a chemisorbed contact barrier [Au−S−C] and physisorbed contact barrier [CH$_3$/Au] or [H/Au], respectively,[15] R_A for the alkyl and conjugated molecular junctions were calculated using eq 5 and are plotted as solid lines in Figure 3. Although it can be found that the R_A values for the experimental, reported, and calculated values are in reasonably good agreement, there are little deviations between reported and calculated R_A values for conjugated molecules. This slight discrepancy may be due to the limitation of the MBT model for conjugated molecules. Also, it could also be because of through-bond transport versus through-space transport. Through-bond transport means the electrons flow along the molecular chains, whereas through-space transport (or chain-to-chain transport) means transport pathways that involve lateral charge hopping between adjacent

molecular chains via intermolecular coupling through van der Waals interactions in an ensemble of the molecules.[23] Although the charge conduction by intermolecular interaction (through-space transport) between molecules is negligible as compared with the dominant through-bond transport,[23,24] the little deviation between the predicted R_A values by the MBT model that considered only through-bond transport and the reported experimental values for conjugated molecules may be because the interaction between π-bonding conjugated molecules can affect more the charge conduction than that of σ-bonding alkyl molecules, as a stronger π−π stacking interaction is expected for aromatic conjugated molecules.[25]

Figure 3 shows R_A (alkyl) > R_A (oligoacene) ≥ R_A (oligophenylene) for a given molecular length, as a result of different molecular body decay coefficients β_{Body} (alkyl) = ~0.92 Å^{-1} > β_{Body} (oligoacene) = 0.50 ± 0.09 Å^{-1} ≥ β_{Body} (oligophenylene) = 0.42 ± 0.07 Å^{-1}, which are based on the experimental observation.[15,19,20] This phenomenon can be explained by the fact that a higher decay coefficient implies faster wave function decay, that is, lower electron transport efficiency (larger resistance), as the β_{Body} value reflects the degree of decrease on the tunneling electron wave function through the molecular structure. There is remarkable difference between alkyl and conjugated molecules in terms of their decay coefficients for charge transport in nonresonant tunneling regime.[10] As compared with a larger HOMO−LUMO gap for alkyl molecules (~8 eV),[6] the smaller gap of conjugated molecules (~5 eV)[26] can explain the lower decay coefficient for conjugated molecules than that for alkyl molecules. Note that here we did not consider the different SAM quality of different molecules. Although the monolayer quality might be different among the different molecules, the quality difference would not be significant enough to cause wrong results in the length dependence transport behaviors among different length molecules.

The contact resistance (R_o) can be defined in the limiting case as d_{Body} approaches zero. However, because R_o depends on the junction area, the specific contact resistance (R_C), the junction area-compensated quantity, is generally obtained and compared among devices with different junction areas, as shown in Figure 4. The results in Figure 4 indicate that (1) R_C (alkanedithiol) is smaller than R_C (alkanemonothiol) roughly by an order of magnitude due to the different properties of chemisorbed and physisorbed contacts side ([CH$_3$/Au] for alkanemonothiol versus [Au−S−C] for alkanedithiol); (2) the R_C difference between
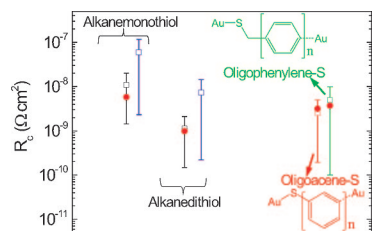
Electronic Conduction in Nonresonant Tunneling Regime

J. Phys. Chem. C, Vol. 112, No. 33, 2008 **13015**

Figure 4. Specific contact resistance R_C for different molecules. The red circles are R_C using the MBT model. The blue, red, and green open squares are R_C values from literature[19,20,22,26] for alkyl, oligoacene thiol, and oligophenylene thiol molecular junctions with Au contacts, respectively. The black open squares are experimental R_C values for alkyl molecular junctions.
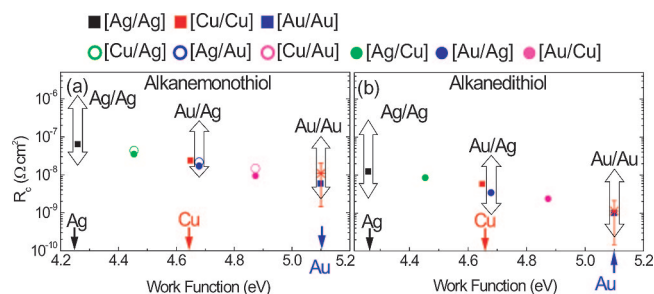

Figure 5. The specific contact resistance R_C for (a) alkanemonothiol and (b) alkanedithiol obtained from the MBT model as a function of metal work function. Open arrows are a range of R_C values estimated from literature.[20,22,26] The red crosses for [Au/Au] are the experimental values obtained in our study.

alkanemonothiol and conjugated counterparts were found to be only different within an order of magnitude due to the difference in the physisorbed contact side ([CH$_3$/Au] for alkanemonothiol vs [H/Au] for conjugated counterparts). However, R_C values for alkanedithiol and conjugated counterparts were calculated to be similar due to the identical chemisorbed contact properties (d_1 and β_C for [Au$-$S$-$C] for chemisorbed contact sides); (3) the R_C between monothiol and dithiol for conjugated molecules were found to be similar due to the comparable properties of chemisorbed and physisorbed contacts side ([H/Au] for mono-thiol vs [Au$-$S$-$C] for dithiol). The R_C values calculated by the MBT model are in good agreement with those obtained from our experiments and reported literature.[20,22,27]

Figure 5 shows the R_C values of various metal$-$molecule contacts (Ag, Cu, and Au) in alkyl M$-$M$-$M junctions obtained from experiment, reported studies, and the MBT model, by assuming tunneling around HOMO, that is, a hole-type tunnel-ing. In Figure 5 the labels are designed such that, for example, [Au/Ag] refers to [Au$-$S$-$(CH$_2$)$_{n-1}$CH$_3$/Ag], that is, the chemi-sorbed contact to the Au electrode and physisorbed contact to the Ag electrode for alkanemonothiol (Figure 5a) or [Au$-$S$-$(CH$_2$)$_n$$-S-$Ag], that is, the chemisorbed contacts to both Au and Ag electrodes for alkanedithiol (Figure 5b). For different metallic junctions (e.g., [Au/Ag], [Ag/Cu], etc.), the average value of the two individual metal work functions was assigned as the work function. As mentioned before, the natures of the chemisorbed and physisorbed contacts are quite different. Because the chemisorbed contacts ([metal$-$S$-$C]) can form strong bondings by molecular overlapping than physisorbed contacts (metal/CH$_3$ or metal/H), generally, the contact decay coefficient for chemisorbed contacts are smaller than that of physisorbed contacts ($\beta_C < \beta_P$), that is, less tunneling electron decay through chemisorbed contacts, as expressed in Table S1 in the Supporting Information. In the MBT model, the contact

decay coefficients (β_C, β_P) in various metallic junctions are dependent on the contact barrier height (Φ_C, Φ_P) and effective mass (α_C and α_P), which can be affected by metal work function, as expressed in eq 8. Note that the contact decay coefficient was observed to decrease when the metal work function is increased. The R_C values were found to be different for asymmetric metal contacts (e.g., [Ag/Au] and [Au/Ag]) for alkanemonothiol because of the different natures of metal$-$molecule contacts (physisorbed vs chemisorbed contact side), as shown in Figure 5a, whereas R_C values for that of al-kanedithiol were found to be same for even asymmetric contacts because of the same nature of metal$-$molecule contact, as shown in Figure 5b. As a result, it was determined that when the average metal work function increases, R_C decreases due to a reduction of the contact barrier height (or contact decay coefficients). The R_C values calculated by the MBT model are in good agreement with those obtained from reported literatures,[20,22,27] as indicated by the red arrows,[15] as shown in Figure 5 and Table S1 (Supporting Information).

Conclusion

We studied the effect of metal-molecule contacts and mo-lecular structures on the electronic transport properties in M$-$M$-$M junctions of alkyl and conjugated molecules of oligoacene and oligphenylene. The resistance, contact resistance, and decay coefficients were obtained and compared for these molecules with different molecular lengths and different metal electrodes, based on a proposed MBT model where the molecular junction was decomposed into three individual barriers through the molecular body and metal$-$molecule contacts on either side of the molecule.

Supporting Information Available: Summary of the contact decay coefficients and specific contact resistances for various M$-$M$-$M junctions calculated from the MBT model (Table S1), Current$-$voltage (I$-$V) characteristics of alkanedithiol (Figure S1a for DC9 and Figure S1b for DC10) and al-kanemonothiol (Figure S1c for C12 and Figure S1d for C16) representative devices, The definition of total lengths, contact lengths, and projected molecular body lengths for alkyl, oligoacene, and oligophenylene molecular junctions for MBT model (Figure S2), Semilog plots of experimental, reported, and calculated resistance per molecule, R_{mol} values for monothiol (Figure S3a) and dithiol (Figure S3b) junctions for three different molecules (alkyl, oligoacene, and oligophenylene) in Au$-$molecule$-$Au junctions, Experimental and calculated parameters α and Φ_B for M$-$M$-$M junctions with Au contacts for alkanemonothiols (Figure S4a) and alkanedithiols (Figure S4b), The overall decay coefficients β_o with molecular length d were calculated from MBT model for alkyl (Figure S4a) and conjugated molecules (Figures S5b and S5c) between Au contacts, and the overall decay coefficients β_o for M$-$M$-$M junctions with various metal contacts for alkanemonothiol and alkanedithiol (Figure S6), This material is available free of charge via the Internet at http://pubs.acs.org.

References and Notes

(1) Reed, M. A.; Lee, T. *Mol. Nanoelectron.*; American Scientific Publishers: 2003.

(2) (a) Aviram, A.; Ratner, M. A. *Chem. Phys. Lett.* **1974**, *29*, 277. (b) Nitzan, A.; Ratner, M. A. *Science* **2003**, *300*, 1384.

(3) (a) Chen, J.; Reed, M. A.; Rawlett, A. M.; Tour, J. M. *Science* **1999**, *286*, 1550. (b) Chen, Y.; Jung, G.-Y.; Ohlberg, D. A. A.; Li, X.; Stewart, D. R.; Jeppesen, J. O.; Nielsen, K. A.; Stoddart, J. F.; Williams, R. S. *Nanotechnology* **2003**, *14*, 462. (c) Stewart, D. R.; Ohlberg, D. A. A.; Beck, P. A.; Chen, Y.; Williams, R. S.; Jeppesen, J. O.; Nielsen, K. A.; Stoddart, J. F. *Nano Lett.* **2004**, *4*, 133. (d) Green, J. E.; Choi, J. W.; Boukai, A.; Bunimovich, Y.; Johnston-Halperin, E.; DeIonno, E.; Luo, Y.; Sheriff, B. A.; Xu, K.; Shin, Y. S.; Tseng, H.-R.; Stoddart, J. F.; Heath, J. R. *Nature* **2007**, *445*, 414.

(4) (a) Selzer, Y.; Salomon, A.; Cahen, D. *J. Phys. Chem. B* **2002**, *106*, 10432. (b) Guisinger, N. P.; Greene, M. E.; Basu, R.; Baluch, A. S.; Hersam, M. C. *Nano Lett.* **2004**, *4*, 55. (c) Xiao, X.; Xu, B.; Tao, N. J. *Nano Lett.* **2004**, *4*, 267. (d) Donhauser, Z. J.; Mantooth, B. A.; Kelly, K. F.; Bumm, L. A.; Monnell, J. D.; Stapleton, J. J.; Price, D. W., Jr.; Rawlett, A. M.; Allara, D. L.; Tour, J. M.; Weiss, P. S. *Science* **2001**, *292*, 2303. (e) Ramachandran, G. K.; Hopson, T. J.; Rawlett, A. M.; Nagahara, L. A.; Primak, A.; Lindsay, S. M. *Science* **2003**, *300*, 1413.

(5) Xu, B.; Tao, N. J. *Science* **2003**, *301*, 1221.

(6) Wang, W. Y.; Lee, T.; Reed, M. A. *Phys. Rev. B* **2003**, *68*, 035416.

(7) Taylor, J.; Brandbyge, M.; Stokbro, K. *Phys. Rev. Lett.* **2002**, *89*, 138301.

(8) Datta, S.; Tian, W.; Hong, S.; Reifenberger, R.; Henderson, J. I.; Kubiak, C. P. *Phys. Rev. Lett.* **1997**, *79*, 2530.

(9) Lindsay, S. M.; Ratner, M. A. *Adv. Mater.* **2007**, *19*, 23.

(10) Salomon, A.; Cahen, D.; Lindsay, S. M.; Tomfohr, J. V.; Engelkes, B.; Frisbie, C. D. *Adv. Mater.* **2003**, *15*, 1881.

(11) Kim, T.-W.; Wang, G.; Lee, H.; Lee, T. *Nanotechnology* **2007**, *18*, 315204.

(12) (a) Akkerman, H. B.; Boer, B. *J. Phys.: Condens. Matter.* **2008**, *20*, 013001. (b) Akkerman, H. B.; Naber, Ronald, C. G.; Jongbloed, B.; Hal, Paul, A.; Blom, Paul, W. M.; Leeuw, Dago, M.; Boer, B. *Proc. Natl. Acad. Sci. USA* **2007**, *104*, 11161.

(13) Lee, J.-O.; Lientschnig, G.; Wiertz, F.; Struijk, M.; Janssen, R. A. J.; Egberink, R.; Reinhoudt, D. N.; Hadley, P.; Dekker, C. *Nano Lett.* **2003**, *3*, 113.

(14) Lee, T.; Wang, W.; Klemic, J. F.; Zhang, J. J.; Su, J.; Reed, M. A. *J. Phys. Chem. B* **2004**, *108*, 8742.

(15) Wang, G.; Kim, T.-W.; Lee, H.; Lee, T. *Phys. Rev. B* **2007**, *76*, 205320.

(16) Simmons, J. G. *J. Appl. Phys.* **1963**, *34*, 1793.

(17) (a) Reddy, P.; Jang, S.-Y.; Segalman, R. A.; Majumdar, A. *Science* **2007**, *315*, 1568. (b) Emberly, E. G.; Kirczenow, G. *Phys. Rev. B* **1998**, *58*, 10911. (c) Taylor, J.; Brandbyge, M.; Stokbro, K. *Phys. Rev. Lett.* **2002**, *89*, 138301.

(18) Rampia, M. A.; Whitesides, G. M. *Chem. Phys.* **2002**, *281*, 373.

(19) Kim, B.; Beebe, J. M.; Jun, Y.; Zhu, X.-Y.; Frisbie, C. D. *J. Am. Chem. Soc.* **2006**, *128*, 4970.

(20) Wold, D. J.; Haag, R.; Rampi, M. A.; Frisbie, C. D. *J. Phys. Chem. B* **2002**, *106*, 2813.

(21) (a) Emberly, E. G.; Kirczenow, G. *Phys. Rev. B* **2001**, *64*, 235412. (b) Hall, L. E.; Reimers, J. R.; Hush, N. S.; Silverbrook, K. *J. Chem. Phys.* **2000**, *112*, 1510. (c) Ventra, M. D.; Pantelides, S. T.; Lang, N. D. *Phys. Rev. Lett.* **2001**, *84*, 979.

(22) Engelkes, V. B.; Beebe, J. M.; Frisbie, C. D. *J. Am. Chem. Soc.* **2004**, *126*, 14287.

(23) Song, H.; Lee, H.; Lee, T. *J. Am. Chem. Soc.* **2007**, *129*, 3806.

(24) Venkataraman, L.; Klare, J. E.; Nuckolls, C.; Hybertsen, M. S.; Steigerwald, M. L. *Nature* **2006**, *442*, 904.

(25) Dou, R.-F.; Ma, X.-C.; Xi, L.; Yip, H. L.; Wong, K. Y.; Lau, W. M.; Jia, J.-F.; Xue, Q.-K.; Yang, W.-S.; Ma, H.; Jen, A. K-Y. *Langmuir* **2006**, *22*, 3049.

(26) Lavrentiev, M. Y.; Barford, W.; Martin, S. J.; Daly, H.; Bursill, R. J. *Phys. Rev. B* **1999**, *59*, 9987.

(27) (a) Beebe, J. M.; Engelkes, V. B.; Miller, L. L.; Frisbie, C. D. *J. Am. Chem. Soc.* **2002**, *124*, 11268. (b) Kaun, C.-C.; Guo, H *Nano Lett.* **2003**, *3*, 1521.